Cerebral Cortex April 2008;18:876–889
doi:10.1093/cercor/bhm126
Advance Access publication July 26, 2007

Subcolumnar Dendritic and Axonal Organization of Spiny Stellate and Star Pyramid Neurons within a Barrel in Rat Somatosensory Cortex

Veronica Egger[1], Thomas Nevian[2] and Randy M. Bruno

Department of Cell Physiology, Max-Planck-Institute for Medical Research, Jahnstr. 29, 69120 Heidelberg, Germany
[1]Present address: Institut für Physiologie der Ludwig-Maximilians-Universität München, Pettenkoferstr. 12, 80336 München, Germany
[2]Present address: Institute for Physiology, Bern University, Bühlplatz 5, 3012 Bern, Switzerland

T.N. performed the measurements on tissue shrinkage and R.M.B. contributed the reconstructions of spiny layer 4 cells filled in vivo and substantial editorial input.

Excitatory neurons at the level of cortical layer 4 in the rodent somatosensory barrel field often display a strong eccentricity in comparison with layer 4 neurons in other cortical regions. In rat, dendritic symmetry of the 2 main excitatory neuronal classes, spiny stellate and star pyramid neurons (SSNs and SPNs), was quantified by an asymmetry index, the dendrite-free angle. We carefully measured shrinkage and analyzed its influence on morphological parameters. SSNs had mostly eccentric morphology, whereas SPNs were nearly radially symmetric. Most asymmetric neurons were located near the barrel border. The axonal projections, analyzed at the level of layer 4, were mostly restricted to a single barrel except for those of 3 interbarrel projection neurons. Comparing voxel representations of dendrites and axon collaterals of the same neuron revealed a close overlap of dendritic and axonal fields, more pronounced in SSNs versus SPNs and considerably stronger in spiny L4 neurons versus extragranular pyramidal cells. These observations suggest that within a barrel dendrites and axons of individual excitatory cells are organized in subcolumns that may confer receptive field properties such as directional selectivity to higher layers, whereas the interbarrel projections challenge our view of barrels as completely independent processors of thalamic input.

Keywords: cortical column, dendritic symmetry, interbarrel projection, intrabarrel confinement, minicolumn, shrinkage

Introduction

In several primary sensory input regions, dendritic arbors exhibit a marked asymmetry, which appears to be closely linked to cortical columns. Dendritic asymmetry is observed most frequently within layer (L) 4, the main target region of thalamocortical afferents, and L2/3, the major subsequent station along the sensory pathway. In visual cortex, several cases of dendritic asymmetry related to borders of cortical columns have been reported (Katz et al. 1989; Hübener and Bolz 1992; Kossel et al. 1995; Elston and Rosa 1997). In the barrel field of rodents, a distinct asymmetric orientation of dendrites away from the barrel borders has been observed, as illustrated in Figure 1; neurons located at barrel centers extend their dendrites in all directions (Lorente de Nò 1922; Woolsey et al. 1975; Steffen and Van der Loos 1980; Simons and Woolsey 1984; Lübke et al. 2000; Staiger et al. 2004). Thus, barrel neurons are apparently subject to intrabarrel confinement. However, all these observations in the barrel cortex were qualitative in nature; here, we provide a quantitative description.

The 2 main excitatory neuronal classes within L4 of somatosensory and visual cortices are spiny stellate neurons (SSNs) and star pyramid neurons (SPNs; Jones 1975; Lund 1984; Martin and Whitteridge 1984; Simons and Woolsey 1984; Hirsch 1995). Their morphological features are similar, except for the apical dendrite of SPNs with a tapered thick trunk that is absent in SSNs. By and large, the similarity also extends to their axonal projections (Lund 1984; Lübke et al. 2000; Staiger et al. 2004). In the barrel cortex, however, SPNs and SSNs appear to differ in dendritic symmetry (Simons and Woolsey 1984; Lübke et al. 2000). Functionally, barrel cortex SSNs and SPNs have been shown to be integrated into different cortical circuits (Schubert et al. 2003), raising the question whether there is an anatomical segregation of SSNs and SPNs within barrels.

Recent work has reinforced the notion of subcolumnar structures or minicolumns (Mountcastle 1978) within a barrel at a functional level: Bruno et al. (2003) have demonstrated the existence of angular tuning domains within a barrel, incorporating neurons that respond preferentially to the same angle of whisker deflection, whereas Andermann and Moore (2006) reported that these domains are arranged in L2/3 such that the direction preference of a barrel neuron is correlated with the somatotopic map. A possible anatomical correlate of minicolumns has been revealed by cytochrome oxidase stainings, although these subbarrels are rather large structures (Land and Simons 1985; Land and Erickson 2005). Moreover, it was observed that axons of spiny L4 neurons are also confined to the respective home barrels at the level of L4, giving rise to the notion of a mostly isolated, intrabarrel excitatory network (Woolsey et al. 1975; Lübke et al. 2000; Petersen and Sakmann 2000, 2001; Brecht and Sakmann 2002a; but see Staiger et al. 2004 for a less pronounced confinement of SPN axons). If functional subbarrel columns would indeed exist, one would predict an even more localized confinement of axons. So the final aim of our analysis was to assess the overlap of axonal and dendritic fields of individual excitatory barrel neurons within the barrel.

These tasks involve several methodological issues. The aforementioned studies on barrel neuron symmetry relied on tangential slices, which allow to relate the position of a neuron within a barrel to the symmetry of dendrites and axon collaterals. The characteristic apical dendrites are, however, often cut or difficult to identify, rendering the classification into SSN and SPN impossible. Thus, we used reconstructions from cells filled in acute thalamocortical slices and from cells filled in vivo to establish symmetry properties of the 2 cell classes in conjunction with their position within the barrel. Next, the bias indices used in the studies of visual cortex neurons are inappropriate to estimate symmetry of barrel neurons in

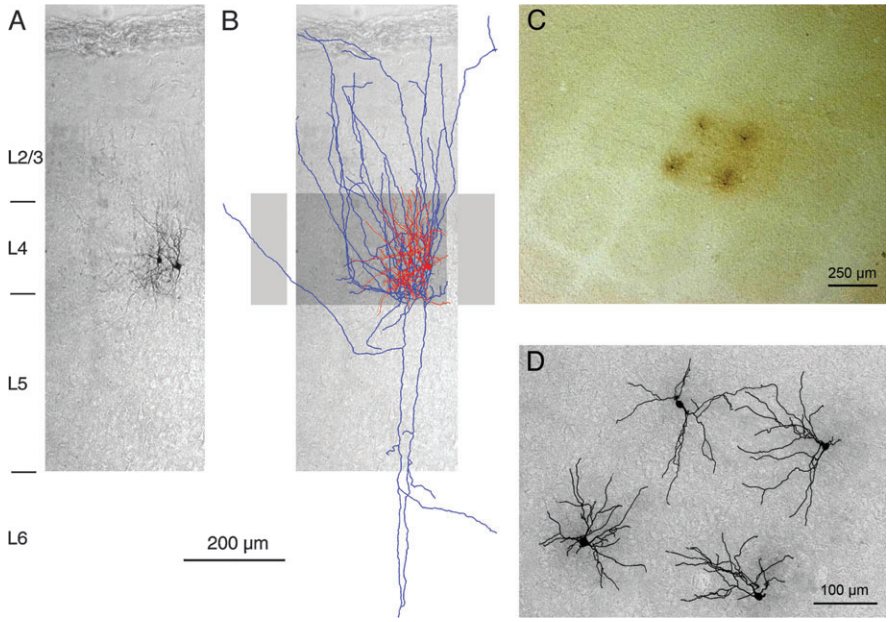

Figure 1. Spiny barrel neurons in thalamocortical and tangential slices. (*A*) Thalamocortical slice with 2 biocytin-stained SSNs. Photograph taken at 10× magnification, cortical layers indicated on the left side. (*B*) Overlay with reconstruction (dendrites red, axons blue) and schematic barrels (gray). Note strong intrabarrel confinement of both dendrites and axons. (*C*) Tangential slice, double stained for cytochrome oxidase as described in the Methods section and with 4 biocytin-stained spiny layer 4 neurons within the corners of a barrel. (*D*) Blow-up of the center part of *C*, overlaid with aligned reconstructions of the dendritic trees.

somatosensory cortex: a bias index is the ratio of the dendritic densities within 2 regions of interest. In many barrel neurons, there are simply no dendrites opposing the main dendritic field orientation and thus more meaningful parameters are required. Finally, in preparations made from acute brain slices there is considerable shrinkage perpendicular to the slice surface, distorting morphological measurements. To properly quantify shrinkage of neurons in our preparation, we compared neuronal morphologies as established with 2-photon microscopy in acute slices to the same biocytin-labeled structures postembedding. The measured degree of shrinkage was then used to estimate its influence on the critical morphological parameters. If applicable, these tools may also be put to use in other cortical areas and central nervous system preparations.

Materials and Methods

Slice Preparation and Filling of Neurons

Thalamocortical slices and tangential slices (350–400 µm; Bernardo and Woolsey 1987; Agmon and Connors 1991; Feldmeyer et al. 1999; Fleidervish et al. 1998) were prepared from the somatosensory cortex of P12–14 old rats. Slices were placed in a recording chamber and viewed with an upright microscope fitted with 2.5× plan/0.075 NA and 40× water/0.80 NA objectives and an additional 4× magnifying lens. The barrel structure of L4 was readily detectable under phase contrast at low magnification. Spiny L4 barrel neurons were selected both on morphological criteria with the aid of infrared video microscopy (Dodt et al. 1998) and their regular spiking firing pattern following depolarizing current injection (Feldmeyer et al. 1999). Whole-cell voltage recordings of spiny L4 neurons were made at physiological temperatures (34–36 °C) using pipettes of 6–9 MΩ with an access resistance below 30 MΩ. The extracellular solution contained (in mM) 125 NaCl, 2.5 KCl, 25 glucose, 25 $NaHCO_3$, 1.25 NaH_2PO_4, 2 $CaCl_2$, 1 $MgCl_2$ bubbled with 95% O_2 and 5% CO_2; the pipette solution contained 105 K-gluconate, 30 KCl, 10 4-(2-hydroxyethyl)-1-piperazineethanesulfonic acid, 10 phosphocreatine, 4 adenosine triphosphate-Mg, 0.3 guanosine triphosphate, adjusted to pH 7.3 with KOH. The osmolarity of this solution was 300 mOsm. Biocytin (2 mg/ml; Sigma, München, Germany) was added to the pipette filling solution for subsequent staining and further identification of the cell type. We also used 19 neurons of P24–35 (mean P29) old rats that were similarly filled in vivo and subsequently recovered from tangential sections. These neurons were published previously (Bruno and Sakmann 2006). See their Supplementary Information for methods.

Histological Procedures

After recording, slices were fixed at 4 °C for at least 16 h in fixative containing 0.1 M phosphate buffer (PB), 2–4% paraformaldehyde and in some cases an additional 1% glutaraldehyde. If slices were stored for longer before processing, the fixative was exchanged with 0.1 M PB after a few days. Biocytin stains were developed as described elsewhere (Horikawa and Armstrong 1988; Lübke et al. 2000). Finally, slices were embedded in Mowiol (Hoechst, Frankfurt, Germany) on a slide mount and coverslipped. Several slices containing biocytin-labeled neurons were double stained for cytochrome oxidase to visualize the position of spiny L4 neuron somata relative to barrel borders, including the in vivo filled cells. A modified version of the classical protocol (Wong-Riley 1979; Wong-Riley and Welt 1980) was used prior to biocytin staining, as described in Feldmeyer et al. (1999). A result of such a double stain of a tangential slice is shown in Figure 1*C*. Moreover, barrel borders can be distinguished to some extent in slices stained normally for biocytin just before the final embedding, although in thalamocortical slices borders may be blurred. The schematic barrel borders indicated in some of the figures were established this way.

Selection of Neurons and Morphological Analysis

Adequately stained small spiny L4 neurons in thalamocortical slices without obviously truncated dendrites were selected and classified according to the following criteria (Lübke et al. 2000): If there was a single, thick apical dendrite (trunk diameter > 2 µm) extending to at least lower L2/3 and with a tapered trunk such that the shape of the soma was slightly triangular (see Fig. 2*B*), the cell was classified as SPN, otherwise as SSN. The third class of excitatory L4 cells, that is, pyramidal cells that are characterized by a skirt of basal dendrites (Jones 1975; Staiger et al. 2004), was not present in our sample, perhaps because we did not label cells near the lower border of L4. For reconstruction and analysis, all SPNs within this sample were used. SSNs were selected at random from the remainder to obtain equal numbers for each class, because they are more numerous within the population (Simons and Woolsey 1984; Feldmeyer et al. 1999). For reconstruction, neurons

were magnified with a 40× or 100× oil/1.3 NA objective fitted to a video microscope. The NEUROLUCIDA system (MicroBrightField, Inc., Colchester, VT) allows a 3-D reconstruction of neuronal structures except for the 2-D representation of the soma. For the computer-aided part of asymmetry and overlap analysis mentioned below, the reconstructed structures were converted to NEURON-readable format. Within NEURON (Hines and Carnevale 1997), 3-D voxel representations of the dendritic and axonal arbors of neurons (see Hellwig 2000) were generated with custom-written software. The origin of the coordinate system was placed to the soma center; a set of voxel representations with different voxel side lengths (1 μm, 5, 10, 15 … 50 μm) was computed. If the distance between 2 subsequent NEUROLUCIDA data points on the same branch was larger than half the chosen voxel side length, additional data points and thus eventually voxels were interpolated. The voxel representation did not account for arbor diameters.

Measuring Asymmetry of Dendritic Trees

To estimate the extent of neuronal asymmetry due to the confinement of the dendritic tree to a barrel, 3-D reconstructions of neurons from thalamocortical slices were rotated with the aid of NEUROEXPLORER (MicroBrightField Inc., Colchester), such that their dendritic tree was projected in the plane parallel to the pia (i.e., the cortical surface), in other words into the barrel field tangential section. This procedure is illustrated in Figure 3*A*. To achieve a proper rotation independent of the cutting angle of the slice preparation, we made use of the fact that the initial part of the axon of SSNs and also SPNs is directed vertically downwards toward the white matter in almost all cases (Woolsey et al. 1975; Lund 1984; Feldmeyer et al. 1999). All other axon collaterals were removed from the reconstruction to avoid confusion. Neurons were rotated until the remaining axon pointed vertically out of the plane of monitor, that is, the viewer looks at the barrel field from the point of view of the white matter. The task of measuring symmetry was thus reduced from 3 to the 2 relevant dimensions. Next, a circle with radius 30 μm was centered at the middle of the soma of the projected neuron. The dendrite-free angle Ɛ was determined as the angular section outside that inner circle that contains no dendrites or at most a single branch without further arborization (Fig. 3*B*). The used size of the circle accounts for the dendrites that first leave the soma in the "wrong" direction and then turn toward the inner of the barrel. Its radius corresponds roughly to one fourth of the average horizontal dendritic field span of spiny neurons (see Table 1). This choice may appear arbitrary, but in the common morphometric Sholl analysis for evaluation of dendritic branching patterns inner circles with comparable radii of 20–40 μm are used (e.g., Sholl 1953; Hübener and Bolz 1992; Elston and Rosa 1997; Mizrahi et al. 2000). In this description, neurons that appear planar in fixed thalamocortical slices due to the shrinkage in the *z*-direction would have an Ɛ-value close to 180°, for example, L2/3 pyramidal cells situated close to the slice surface. Ɛ-values of truly asymmetric neurons should be significantly larger than that, whereas radially symmetric neurons from tangential slices would usually yield values smaller than 90° (see below).

As a more general index for asymmetry of neurons in thalamocortical slices we used the length of the vector between soma center and center of gravity (similar to the vector mapping in Tailby et al. 2005), which was calculated using a fine voxel representation of the dendritic tree. This representation was generated as described above, with a voxel side length of 1 μm. Our aim was to measure symmetry with respect to the barrel cross section. Thus, prior to the distance calculation the center of mass was projected into the plane defined by the initial axon part (representing the normal vector), that is, into the projection plane used previously for the determination of Ɛ. Neither dendritic diameters nor the soma volume was taken into account.

Measuring Axonal Symmetry and Overlap between Dendritic and Axonal Fields within L4

To investigate the overlap between dendritic and axonal fields of neurons with a fully stained axonal tree, this procedure was then repeated with an axonal tree pruned such that it retained all collaterals within L4. In order to ensure proper rotation, the first projection described above was used as a template, because the initial part of the axon is often no longer clearly discernible within the tree structure. The axon-free angle Ɛ was thus determined for the axonal tree reduced to L4. To estimate the overlap between dendritic and axonal tree of the same spiny barrel neuron, the fraction of volume taken up by both axonal and dendritic segments was determined with the aid of coarse voxel representations (see above). Upon comparison of representations with increasing voxel side length (5, 10, 15… μm), the appropriate voxel side length for this analysis appears to be in the range of 20–25 μm (see Results section). The overlap is given as fraction of dendritic voxels.

Coordinate Systems and Shrinkage Definition

Relative to the Slice

Here, the coordinates are *x*, *y*, *z* with the *z*-axis perpendicular to the slice plane, and the *x*- and *y*-axes within the slice plane. In Figure 2*A* the coordinate system is shown both for the thalamocortical and tangential slice preparation. Thus, the shrinkage effect perpendicular to the slice plane is called *z*-shrinkage, in short S_z. It is defined as shrunk length z_s divided by original length z_0 and thus equivalent to the linear factor known from anatomical studies (e.g., Hellwig 2000).

Relative to the Barrel Field

Horizontal/tangential and vertical are the directions relative to the barrel field, with vertical being perpendicular to the whole whisker map.

Measurement of Shrinkage

Shrinkage within the slice plane (*xy*-shrinkage, S_{xy}) and perpendicular to the slice plane (S_z) was estimated by comparing the morphology acquired from 2-photon fluorescence stacks of 4 spiny stellate cells filled with 50 μM Alexa 594 (Invitrogen, Carlsbad, CA) and biocytin in acute slices to the morphology after biocytin labeling and postembedding. Two-photon fluorescence image stacks were acquired with a confocal scanning unit (LFS SP2RS, Leica Microsystems, Mannheim, Germany) attached to an upright microscope (DMLFS; Leica) equipped with a 63× objective and a Ti:Sa-Laser (MIRA 900F, pumped by a 5W Verdi; Coherent, Santa Clara, CA) (Nevian and Sakmann 2006). Fluorescence stacks were analyzed using ImageJ.

Table 1
Morphological parameters of neurons reconstructed from thalamocortical slices

	SSNs (n = 21)			SPNs (n = 22)			SSN versus SPN
	Mean	SD	Range	Mean	SD	Range	P
Caliber of most vertical/apical dendrite (μm)	1.6	0.4	0.9-2.7	3.2	0.6	2.4-4.4	<0.001
Length of most vertical/apical dendrite (μm)	119	59	58-270	152	59	92-365	<0.1
Vertical dendritic field span (μm)	195	39	130-303	235	80	86-486	<0.1
Horizontal dendritic field span (μm)	138	38	86-225	196	52	120-326	<0.001
Maximal horizontal dendritic length (μm)	108	20	67-156	116	31	67-196	>0.2
Maximal dendrite-free angle ε (°)	245	42	183-306	162	26	80-199	<0.001
Center of gravity distance to soma (μm)	29	10		20	8		<0.05

Note: Morphological parameters of reconstructed SSN and SPN dendrites. For trunk caliber measurement and orientation of field spans see also Figure 2, for measurement of the maximal dendrite-free angle see Figure 3. The maximal horizontal dendritic length was the extension of the longest single dendrite of the neuron. The center of gravity distance to the soma was measured based on a voxel representation of the neurons (see Methods); apparently it is not particularly well suited as a simple measure of neuronal symmetry. The significance of differences between SSN and SPN shown in the last column was tested using the 2-tailed, unpaired Student's *t*-test.

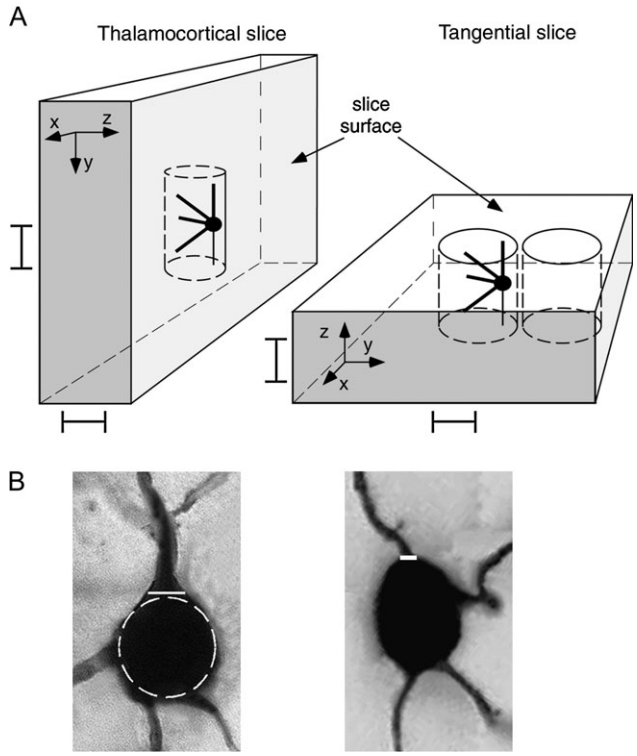

Figure 2. Coordinate systems in thalamocortical and tangential slices and measurement of the (trunk) diameter of the apical/uppermost dendrite. (*A*) Thalamocortical slices cut vertically through barrels, tangential slices through their cross section. In both slice types, barrels and the same asymmetric neuron are schematically represented, with the axon being the thin downward branch. The *xyz*-system is defined by the reconstruction software. The *z*-axis corresponds to the focus of the reconstruction microscope and is thus always perpendicular to the slice surface. Vertical and horizontal are directions relative to the barrel field: Vertical is in the direction of the pial surface and horizontal applies to the tangential cross section of the barrel field. In the scheme, vertical and horizontal field spans in both slice types are indicated by the thick bars. (*B*) Photomicrographs of somatic regions of a SPN and a SSN, taken at 100× magnification. Measured diameters of apical trunks and uppermost dendrites, respectively, indicated as white bars, and the circle used in case of triangularly shaped somata as white broken line (see Methods). Scale: width of photomicrographs 25 μm.

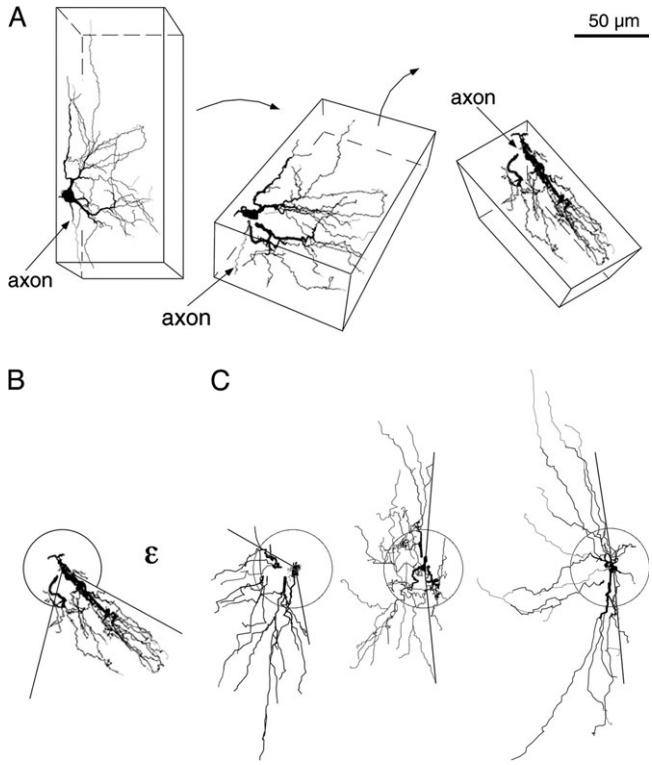

Figure 3. Symmetry properties of spiny layer 4 neurons. (*A*) Rotation of a neuron from the thalamocortical slice plane (original reconstruction) into the tangential plane. Only the initial part of the axon is shown in light gray. Rotation is performed such that the axon points vertically out of the drawing plane (from left to right). The soma is now almost invisible, because it is reconstructed in 2-D (see Methods). The neuron used for this illustration was classified as spiny stellate cell. The scale bar applies to the entire figure. (*B*) In the tangential plane, the dendrite-free angle is defined as the angular section ε that contains no dendrites (or just one single branch) outside of a circle with radius 30 μm. (*C*) Three additional projected neurons are shown, another SSN on the left side and 2 SPNs on the right side. Circles with radius 30 μm and dendrite-free angles are indicated.

Estimate of Shrinkage Distortion of the Dendrite- or Axon-Free Angle

Considerable *z*-shrinkage S_z may distort the symmetry measurements especially in thalamocortical slices. This is illustrated schematically in Figure 8*A*. As a first approximation, S_z is assumed to be homogenous within the slice. Because this problem is independent of the angle φ between a dendrite and either the *x*- or *y*-axis in the *xy*-plane, cylindrical coordinates are used with $r^2 = x^2 + y^2$, and each dendritic tip can be described by the coordinates (z, r, φ). As illustrated in Figure 8*C*, left panel, the *r*-coordinate of a dendrite with initial length L is conserved because there is no *xy*-shrinkage (see Results). But the *z*-coordinate shrinks from z_0 to z_s, causing an overall reduced length of the dendrite L_s. The amount of shrinkage depends on the relative orientation of the dendrite with respect to the *z*-axis, as shown for all possible orientations in Figure 8*C*, right panel.

$$L^2 = r^2 + {z_0}^2;\ S_z = \frac{z_s}{z_0} \Rightarrow {L_s}^2 = r^2 + {z_s}^2 = r^2 + {S_z}^2(L^2 - r^2) \qquad (1)$$

The influence of S_z on the angle α between a dendrite and the slice plane normal (Fig. 8*D*, left) can be estimated by introducing the shrunk dendritic length L_s into the following expression for the angle α (eq. 2). In the case of the overall dendritic orientation drawn in Figure 8*A*, both the dendrites that enclose the largest dendrite-free angle extend toward the slice surface. In the course of shrinkage these dendrites will be bent away from the slice plane normal (i.e., the *z*-axis), therefore twice the squeezing of α will result in an upper limit for the change ΔΕ that could be induced by shrinkage (eq. 3). Figure 8*D* shows the estimated dependency of ΔΕ on the dendritic length, given our measurements of L in tangential slices and S_z (see Results).

$$\cos\alpha = \frac{r}{L} \overset{\text{(eq.1)}}{\rightarrow} \cos\alpha_s = \frac{r}{L_s(r)} = \frac{r}{\sqrt{r^2 + {S_z}^2(L^2 - r^2)}} \qquad (2)$$

$$\Delta\varepsilon \geqslant 2(\alpha - \alpha_s) = 2\left(\arccos\left(\frac{r}{L}\right) - \arccos\left(\frac{r}{L_s(r)}\right)\right) \qquad (3)$$

In terms of shrinkage distortion the case underlying the above estimate represents the worst-case. In any other arrangement—one or 2 of the dendrites that include Ε being directed away from the slice surface—the distortion would be smaller because these dendrites would be bent toward the dendrite-free section and therefore counteract the increase in Ε. Thus, one may also argue that there is a bias in shrinkage distortion with respect to cell type: Radially symmetric neuron reconstructions probably suffer from a stronger increase in Ε than asymmetric neurons because in symmetric neurons the probability of *both* outermost dendrites (that enclose Ε) being directed toward the surface is larger.

Measurement of Field Span and Caliber of the Uppermost Dendritic Trunk

The thick bars within the schematically drawn slices in Figure 2*A* denote the respective horizontal and vertical field spans. In the thalamocortical preparation the vertical field span corresponds to the extension of the dendritic field in the *z*-direction, and the horizontal

field span to its spread in the plane spanned by the *x*- and *y*-axes. To determine the caliber of the trunk of the apical/uppermost dendrite, the diameter of the uppermost dendrite emerging from the soma was measured right at the branchpoint from the soma that was approximated to be of spherical shape. Figure 2*B* shows an example of a SPN and SSN uppermost dendrite and the trunk diameter measurement.

Measurement of the Position of a Neuron Relative to the Barrel

In tangential slices, the distance of neuronal somata from the next barrel wall was also measured and normalized by the barrel diameter. For every cell, the barrel diameter was measured by taking the wall-to-wall-distance that would run through the soma of the cell along the direction of rows within the barrel field. Neurons were classified as barrel wall neurons if their somata were found within the outer two fifths of a barrel, that is, had a fractional distance of less than 0.40 from the barrel border to the center; otherwise they were classified as barrel center neurons (see also Fig. 4*E*).

Mean values are given ±SD. A 2-tailed, unpaired Student's *t*-test was applied to test for significance levels.

Results

Dendritic Symmetry of L4 Neurons in Thalamocortical Slices

The spatial extension of the dendritic field of SSNs, for example, in the visual cortex has been characterized as spherical and radially symmetric, hence the name "stellate cell" (Lorente de Nò 1922; Lund 1984). In contrast to this symmetric distribution of dendrites within all directions in space, rat barrel cortex SSNs characteristically show an asymmetric, eccentric dendritic field (Fig. 1). This asymmetric orientation appears to be due to their confinement to single barrels (Woolsey et al. 1975; Steffen and Van der Loos 1980; Simons and Woolsey 1984). However, the second class of small spiny L4 barrel neurons, the SPNs, does not show a similarly strong deviation from radial symmetry.

The distinction between SSNs and SPNs was based on the presence of a thick apical dendrite (see Methods). A few neurons with relatively long uppermost dendrites lacked a tapered thick trunk and thus were classified as SSNs, although they may represent an intermediate form that belongs to the proposed continuum between the 2 cell classes (Jones 1975; Lund 1984). However, their removal from the sample did not significantly change the main results.

To measure neuronal asymmetry, we devised a method that is adapted to the morphological features of spiny L4 neurons within barrels (described in detail in the Methods section). Figure 3*A* shows the rotation of 3-D reconstructions of spiny L4 neurons from thalamocortical slices, such that their dendritic tree was projected in the plane parallel to the cortical surface. This projection is independent of the slice angle because the initial part of the axon of spiny L4 neurons projects vertically to the white matter (Lorente de Nò 1922; Woolsey et al. 1975; Lund 1984; Feldmeyer et al. 1999). For clarity, all other axonal collaterals were removed from the reconstruction. The task of quantifying symmetry was thus reduced from 3 to the 2 relevant dimensions. Projections of the 2 neuronal types are shown in Figure 3*B,C*. In the projection, the dendrite-free angle Ɛ was determined as the angular section outside an "inner circle" drawn around the soma (radius 30 μm, Fig. 3*B*), which contains either no dendrites or just one single branch.

In addition, the vertical and horizontal field spans and the horizontal span of the longest dendrite were measured (see Methods, Fig. 2*A,B*). Finally, the center of gravity within the projection plane was determined.

Differences in Dendrite-Free Angle

The data measured from SSNs and SPNs in thalamocortical slices are summarized in Table 1. The measurement of the dendrite-free angle of SSNs confirms the impression of strong asymmetry: The dendrite-free angular section Ɛ of 21 SSNs within the horizontal plane ranged from 183° to 306° (mean 245 ± 42°). Conversely, the eccentricity of the dendritic field measured for 22 SPNs is far less pronounced, their mean dendrite-free angular section being Ɛ = 162 ± 26°, ranging from 80° to 199° (see Fig. 3*C*). This difference in asymmetry between the 2 cell classes is also reflected in the horizontal field span, with SPNs exceeding SSNs by ~40%, because in a radially symmetric neuron there are opposed dendrites adding up to the field span, that are absent in asymmetric neurons. Moreover, the difference in field span is not due to a difference in the maximal horizontal span of single dendrites as these values are similar.

The difference in dendrite-free angle and thus symmetry appear not to change with further development, because the difference between SSNs and SPNs in older animals is about 88° (around P29; $n = 9$ vs. $n = 10$; $P < 0.005$), similar to younger ones.

SPNs have slightly triangular somata of a size similar to that of the round somata of SSNs. Unlike most of the other dendrites, their apical dendrite has a tapered trunk and an initial part twice as thick as that of dendrites emerging from the upper part of SSNs (see Figs 2*B*, 7*A*). However, it has to be emphasized that this apical dendrite is much less pronounced than its counterparts of L5 or L2/3 pyramidal neurons because it lacks a tuft and does not extend to reach L1. Its average length exceeds that of the uppermost dendrite emerging from SSNs by only ~25%.

Figure 4*A,B* summarizes the symmetry properties of both SSN and SPN dendrites in thalamocortical slices. The dendrite-free angle Ɛ is plotted against the caliber of the initial segment of either apical dendrite (SPNs) or the dendrite closest to the vertical top of the soma in the case of SSNs and against the ratio of horizontal single dendrite to field span. Figure 4*A* shows the codependence of symmetry and the existence of a thick apical dendrite, which served as main criterion for classifying the neuron as SPN.

Taken together, an additional criterion for distinction between SSNs and SPNs in barrel cortex emerges: Whenever a spiny L4 barrel neuron has a strongly asymmetric dendritic field, it is probably a SSN, whereas radially symmetric fields are more characteristic for SPNs.

Dendritic Symmetry of Neurons in Tangential Slices from In Vitro and Vivo Fillings

An example of a tangential slice with 4 stained neurons located at the "corners" of a barrel is shown in Figure 1*C,D*. Neurons were classified as barrel wall or barrel center neurons according to the relative distance of their soma to the outer barrel border (see Methods). The mean dendrite-free angular section Ɛ of 18 barrel wall neurons in tangential slices from both in vitro and in vivo fillings was 175 ± 54° whereas 16 barrel center neurons had a much smaller dendrite-free section of 79 ± 50° ($P < 0.001$; Fig. 4*E*). The considerably smaller dendrite-free sections in tangential versus thalamocortical slices (see Table 1) can be explained by the influence of shrinkage (see below). These data indicate that barrel wall neurons are preferably eccentric and barrel center neurons preferably radially symmetric, which corresponds to the earlier finding of intrabarrel confinement. Given our previous observation of symmetries of SSNs and SPNs in thalamocortical slices, one might conclude that this preference is

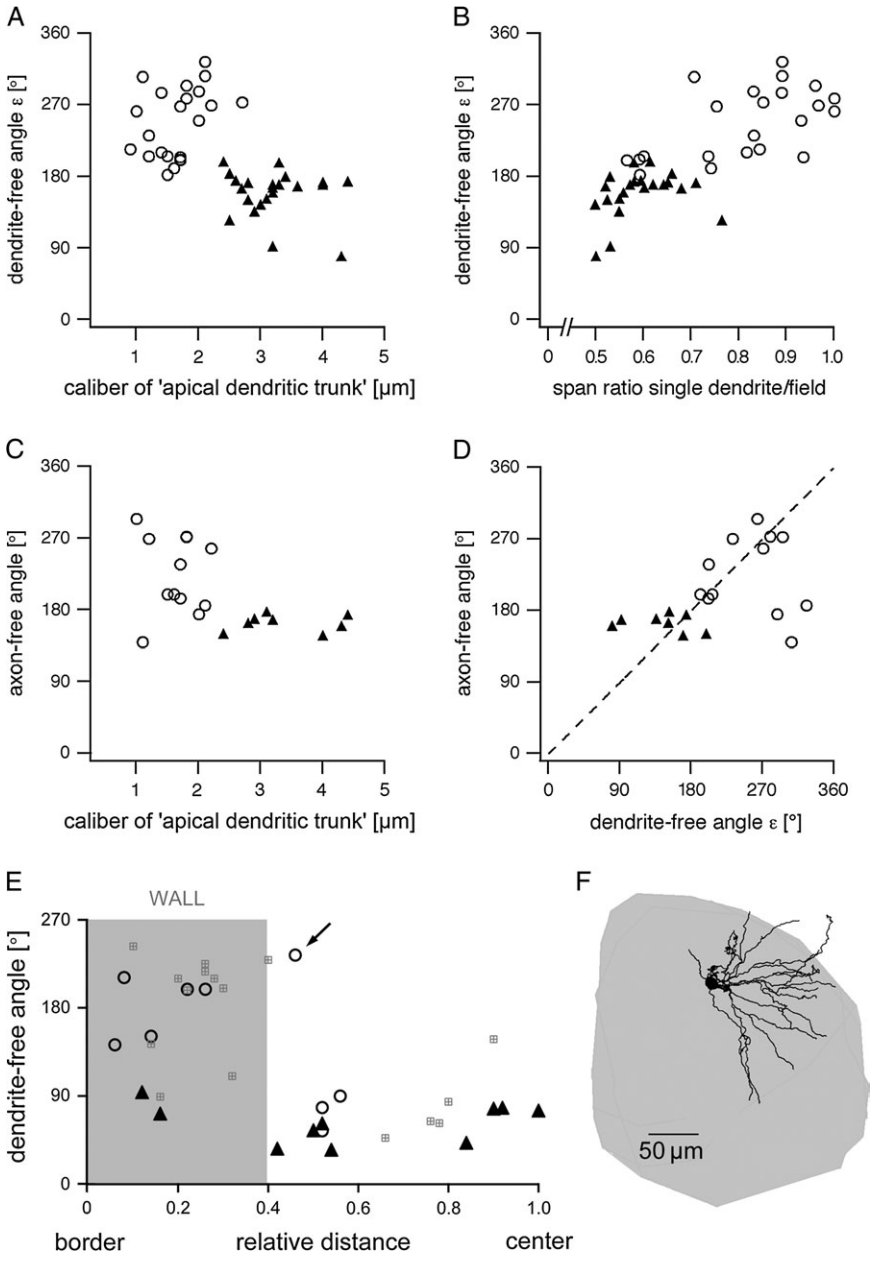

Figure 4. Symmetry measurements in thalamocortical and tangential slices. In all graphs, closed triangle represents SPNs and open circle SSNs. (*A*) The dendrite-free angle ε of spiny L4 neurons reconstructed from thalamocortical slices is plotted versus the caliber of the trunk of their apical dendrite, if they were SPNs ($n = 22$), and versus the caliber of their uppermost dendrite, if they were SSNs ($n = 21$; for the measurement (see Fig. 2*B*). (*B*) Here the dendrite-free angle ε is shown versus the ratio of the horizontal span of the longest single dendrite (within the projection plane) to the horizontal span of the whole dendritic field. (*C*) Same type of graph as in (*A*), but for axon collaterals. Here the axon-free angle is shown versus the caliber of the trunk of the apical dendrite in the case of SPNs ($n = 8$), and versus the caliber of the uppermost dendrite for SSNs ($n = 12$). (*D*) The axon-free angle is shown versus the dendrite-free angle ε of spiny layer 4 neurons. The broken line indicates a ratio of 1:1. (*E*) The dendrite-free angle ε of spiny layer 4 neurons reconstructed from acute tangential slices (gray squares, $n = 15$) and of identified SSNs and SPNs reconstructed from in vivo fillings ($n = 9$ and $n = 10$) is shown versus the relative distance of the neurons from the barrel border. The barrel border on the left end of the *x*-axis thus corresponds to a relative distance of 0, the barrel center on the right end to 1. The SSN outlier shown in (*F*) is marked by a black arrow. (*F*) Unusual SSN: This neuron is asymmetric, but its dendrites are oriented away from the barrel center, toward the border. This is the only asymmetric cell in our sample ($n = 39$) that shows this kind of dendritic orientation.

also mirrored in the cell type, with SSNs located mostly at the barrel wall and SPNs mostly at the center. However, when looking at the completely reconstructed set of neurons that was recovered from in vivo fillings, where the presence of an apical dendrite allows for further classification, this notion does not hold for all neurons (Fig. 4*E*; see Discussion). Nevertheless, the barrel wall is mostly populated by asymmetric SSNs and the barrel center mainly by symmetric SPNs. The latter finding is also illustrated by Figure 7*A*, showing a cluster of 5 SPNs within the barrel center.

All asymmetric cells in our sample including thalamocortical and tangential slices and neurons reconstructed from in vivo fillings ($n = 39$) had their dendrites oriented away from the barrel border, in accordance with the previously reported intrabarrel confinement—with the exception of the SSN shown

in Figure 4*F*. Perhaps this cell is confined to a subbarrel (Land and Erickson 2005).

Symmetry of Axons and their Overlap with the Dendritic Field in L4

Although axonal structures are difficult both to recover and resolve for reconstruction from acute tangential slices, thalamocortical slices allow for their reconstruction and subsequent analysis with respect to symmetry properties and overlap with dendritic structures. The axons of spiny L4 neurons typically were found to span all cortical layers, with their collaterals most dense in L4 and lower L2/3; their orientation within these layers is mainly vertical, and at the level of L4 the axonal arbor appears to be confined to a single barrel, similar to the dendritic field (Woolsey et al. 1975; Feldmeyer et al. 1999; Lübke et al. 2000; Petersen and Sakmann 2000, 2001). Here, this observation was confirmed by measuring the asymmetry of the axonal arbor exclusively within L4. Moreover, the overlap between dendritic and axonal field was calculated (Methods). These data are summarized in Table 2.

An example of extensive overlap is shown in Figure 5*A,B*. For SSNs, the mean axon-free angle in L4 amounts to 225 ± 49°, only slightly smaller than their dendrite-free angle of 245 ± 42°. Thus, SSN axon collaterals are almost as eccentric as their dendrites. The axon-free angle of SPNs is also similar to their dendrite-free angle. The relation between the axon-free angle and the cell class shown in Figure 4*C* resembles the relation between dendrite-free angle and cell class described above. In the projection plane, axon- and dendrite-free angles closely overlapped in all cases and for both neuronal classes (Fig. 4*D*).

Overlap Analysis

Because the overlap between dendritic and axonal voxels within L4 increases linearly with voxel side length until 20–25 μm as illustrated in Figure 5*C*, a voxel side length of 25 μm represents a plausible choice for the overlap analysis. Moreover, it is on the order of magnitude of distance intervals commonly used for Sholl analysis. For SSNs, the overlap is within 70 ± 15% of dendritic voxels, whereas SPNs display this overlap to a lesser extent (47 ± 14% of dendritic voxels, Fig. 5*C* upper 2 panels). This difference in overlap was not due to a reduced density or extent of dendritic and axonal branches, because there were more elementary axonal and dendritic voxels with side lengths 1 and 25 μm in SPN than in SSN (see Table 2).

This strong overlap between dendrites and axons is a hallmark of L4 barrel neurons that is not displayed by cortical pyramidal neurons: Reconstructed L5 and 2/3 pyramidal neurons with well-filled axons were selected from our local database. The overlap difference between neurons from the 2 layers was insignificant, thus results were pooled. At a voxel side length of 25 μm, there was an overlap in 15 ± 6% of dendritic voxels in pyramidal neurons (n = 12, Fig. 5*C* bottom, $P < 0.001$ vs. both SSNs and SPNs). If the apical dendrite was not taken into account, overlap increased to 30 ± 8% but was still significantly smaller ($P < 0.001$ vs. SSNs and $P < 0.05$ vs. SPNs).

Interbarrel Projection Patterns

Previous studies have shown that similar to dendrites, axons of spiny L4 neurons are subject to intrabarrel confinement at the level of L4 (Woolsey et al. 1975; Lübke et al. 2000; Petersen and Sakmann 2000, 2001), although SPN axons tend to extend into the immediately adjacent walls of the surrounding barrels (Staiger et al. 2004). However, 3 exceptions to this generalization were found which had clear interbarrel projections. Figure 6 shows 2 SSNs with an axonal projection to an adjacent barrel and the region in L2/3 above it. Even these neurons are clearly confined with respect to the home-barrel border. Their interbarrel projections target roughly the same region within the adjacent barrel as the intrabarrel projection. Figure 7 shows the axonal projections of 3 SPNs clustered at the barrel center; one cell projects to the centers of 2 adjacent barrels, although the projection is not dense. A similar SPN projection pattern has been reported previously (Brecht and Sakmann 2002a).

Measurement of z-Shrinkage and its Influence on the Dendrite-Free Angle ε

Given the substantial degree of z-shrinkage in the slice preparation, it is important to assess its influence on symmetry measures and therewith the reliability of our conclusions. By comparing morphologies of the 4 same L4 neurons within the acute slice acquired with 2-photon microscopy and the embedded preparation, the average z-shrinkage S_z was determined to be 0.45 ± 0.10 (n = 32 distances between structures in the 4 cells; Methods), whereas the planar shrinkage S_{xy} was negligible (n = 21; both Fig. 8*B*). This low degree of S_{xy} is in the same order of magnitude as S_{xy} previously observed in comparable brain slice preparations (e.g., Hellwig 2000). Therefore, we

Table 2
Axon analysis and overlap axon-dendrite of individual L4 neurons

	SSNs (n = 12)		SPNs (n = 8)		SSN versus SPN
	Mean	SD	Mean	SD	P
Axon-free angle (°)	225	49	164	11	<0.005
Mean overlap (fraction of dendritic 25-μm voxels) (%)	70	15	47	14	<0.05
Mean number of dendritic 1-μm voxels	2055	731	2402	830	>0.1
Mean number of axonal 1-μm voxels (in L4)	4782	2288	4931	2824	>0.5
Mean number of dendritic 25 μm voxels	55	16	78	13	<0.01
Mean number of axonal 25-μm voxels (in L4)	144	68	150	85	>0.5
Dendritic "barrel fill factor" (25-μm voxels) (%)	7–15		10–25		
Axonal "barrel fill factor" (25-μm voxels) (%)	20–45		25–50		

Note: All data were measured from neurons in thalamocortical slices, with the axonal reconstruction pruned to collaterals within L4. The axon-free angle was determined as for the dendrite-free angle. For generation of the voxel representations, see Methods. The overlap is defined here as the fraction of dendritic voxels that coincide with axonal voxels of the same neuron (voxel side length 25 μm, see Methods and Results). The "barrel fill factor" was estimated based on the following assumptions: A barrel is ~200 μm in height, and 200–400 μm in diameter depending on its location within the barrel field (Simons and Woolsey 1984). Due to the described shrinkage effects (see Results, Methods) it is reasonable to assume a barrel volume reduction of ~50% for neurons recovered from thalamocortical slices, resulting in a barrel volume of ~0.005–0.01 mm^3. Similar to the overlap analysis, a voxel side length of 25 μm and hence a volume unit of 15.6×10^{-6} mm^3 was used. N as listed in the top row, except for the mean number of dendritic 1-μm voxels (n = 21 and 22, respectively).

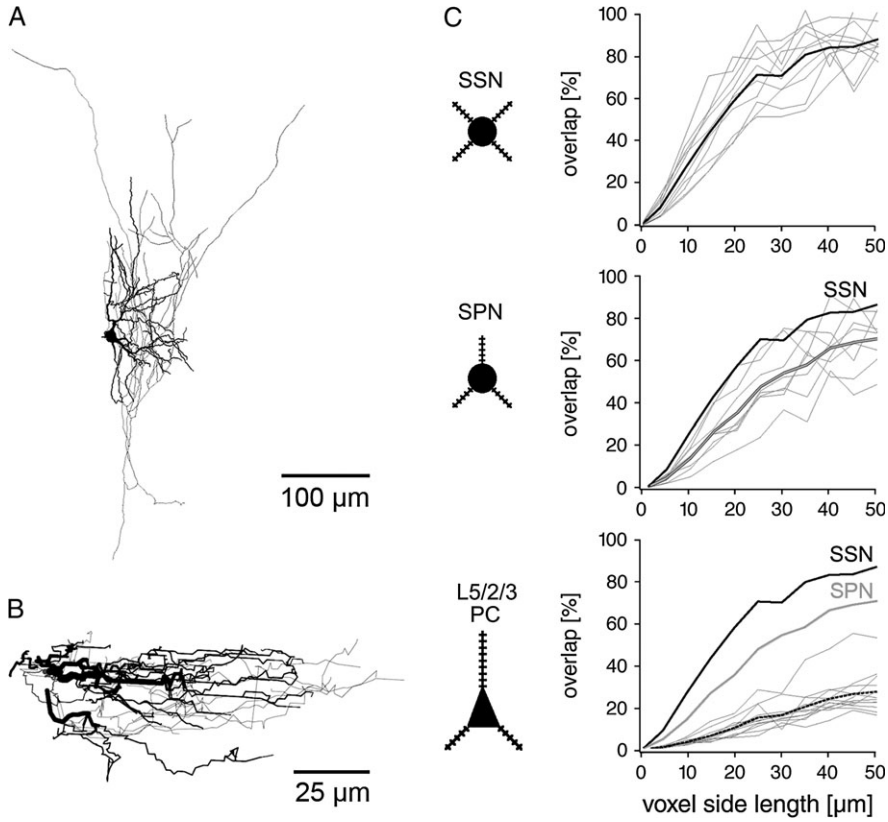

Figure 5. Axonal confinement and overlap with dendritic tree. (*A*) Reconstructed neuron in thalamocortical slice. Same neuron as in Figure 2, but shown with axonal projection (thin lines). (*B*) The same neuron projected into the tangential plane. Before rotation, the axon collaterals were pruned such that they retained only their branches within layer 4. The projection without collaterals shown in Figure 2B was used as a template to enable proper rotation. (*C*) The overlap between dendritic and axonal volume elements is estimated by comparing 3-D voxel representations of dendritic and axonal trees (see Methods). In the graphs, the overlap (in percent of dendritic voxels) is shown depending on the voxel side length of the representations. Thin gray lines represent single neurons. The top graph shows data from 12 SSNs and their average (thick black line). The middle graph shows data from 8 SPNs, the SPN average (gray thick line) and the SSN average (black thick line). The bottom graph includes data from 6 L2/3 and 6 L5 pyramidal neurons, their average (thick black broken line), and both the SSN average (black thick line) and the SPN average, as shown above (gray thick line).

neglected S_{xy} in all further considerations. Although Figure 8*B* shows a certain nonlinearity in S_z—in all cells S_z was stronger close to the slice surface and decreases with depth—we assume a linear S_z to estimate its effect on the dendrite- or axon-free angle: The maximal artifactual increase in ε due to a S_z of 0.45 would amount to on average $\Delta\varepsilon \approx 33°$ and maximally $\Delta\varepsilon \approx 45°$ (see Methods eq. 3, Fig. 8*D*). In conclusion then, although there is considerable *z*-shrinkage, its influence on symmetry does not compromise the observation of different dendritic symmetries between SSNs and SPNs, because the average difference in dendrite-free angle $\Delta\varepsilon$ of 83° between the 2 classes (Table 1) is roughly twice the maximal estimated $\Delta\varepsilon$ as caused by shrinkage.

Discussion

Here, we have quantified dendritic symmetry of the 2 main excitatory neuronal classes within L4 of rat barrel cortex; SSNs and SPNs. SSN had mostly eccentric morphology, whereas SPNs were nearly radially symmetric. Most asymmetric neurons were located near the barrel border. The axonal projections within L4 were largely restricted to a single barrel except interestingly for those of 3 interbarrel projection neurons. Dendritic and axonal fields closely overlapped, being more pronounced in SSNs versus SPNs and considerably stronger in spiny L4 neurons versus extragranular pyramidal cells. Thus, dendrites and axons of individual excitatory barrel cells appear to be organized in subcolumns that further determine the organization of RF properties across L2/3.

Methodological Aspects: Asymmetry Measures and Shrinkage Distortion

To capture the asymmetry of spiny L4 neurons, we measured the dendrite-free angle of the projection of the neuron into the tangential plane relative to the barrel field. This simple and efficient measure could be easily extended to axonal structures. The previously mentioned measures of dendritic asymmetry used in visual cortex (i.e., bias indices; Katz et al. 1989; Hübener and Bolz 1992; Kossel et al. 1995) are not applicable to asymmetric barrel cortex neurons because of their extremely eccentric field. Polar plots that depict the number of dendritic intersections or coverage per angular section, appear to be another suitable means to characterize dendritic asymmetry (e.g., Leventhal and Schall 1983; Elston and Rosa 1997; Staiger et al. 2004). However, such plots simplify the neuronal structure only to some extent and therefore cannot be easily analyzed and/or classified. Furthermore, the comparison of neurons that are located in different corners of the barrel would require suitable normalization procedures.

In acute slice preparations, the processing and embedding causes slices to shrink mainly in the *z*-direction, that is, perpendicular to the slice plane. Shrinkage reduces the extension

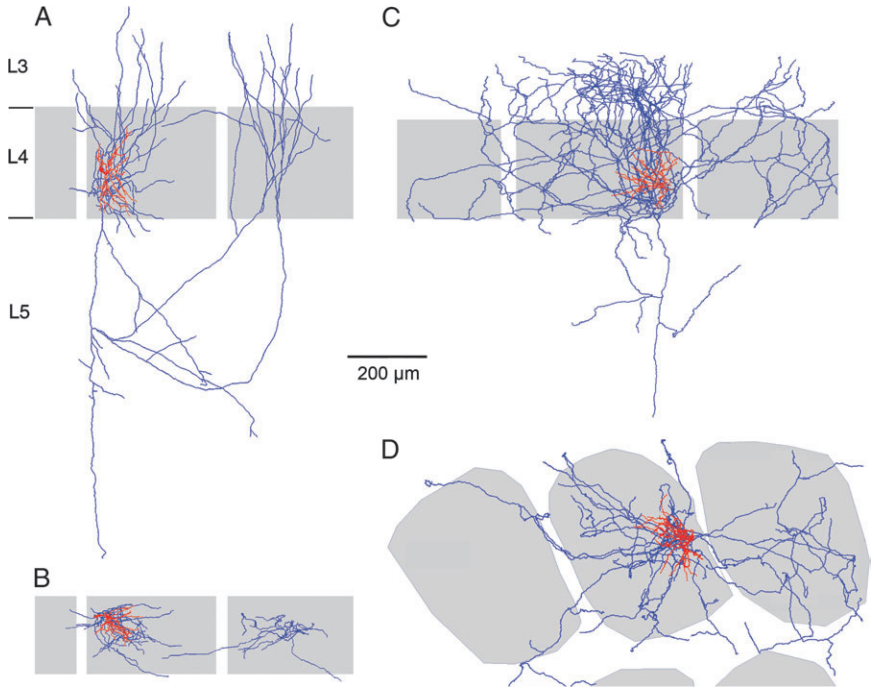

Figure 6. Interbarrel projection of 2 SSNs. (*A*) SSN with interbarrel projection as reconstructed from a thalamocortical slice (age of animal P12). Dendritic tree red, axon blue. Schematic barrels are indicated in light gray. The adjacent barrels are located within the same row. The scale bar applies to all reconstructions. (*B*) Projection of the above neuron into the tangential plane with the axon collaterals reduced to L4. Schematic barrels are indicated in light gray. The projection to the adjacent barrel is almost as dense as the intrabarrel projection, at least in terms of voxels with side length 1 µm (4900 vs. 7500) and 25 µm (165 vs. 203, compare also with values in Table 2). (*C*) SSN with very extensive axonal arborization and interbarrel projection as reconstructed from an in vivo filling (age of animal P30). Dendritic tree red, axon blue. Barrels are indicated in light gray. The interbarrel projection is directed toward an adjacent barrel in the same row D. In comparison with the SSN shown in (*A*), this SSN is squeezed in the vertical axis due to *z*-shrinkage. (*D*) Projection of the above neuron into the tangential plane with its axon collaterals reduced to L4. Barrels are indicated in light gray.

of neurons in this direction by about one half. Unfortunately, it is not possible to correct properly for this effect due to its nonlinearity: According to our direct comparison of neuronal structures pre- and postembedding, shrinkage is strongest in the region closest to the surface. This might be caused by various factors. First, cells at the slice surface die and therefore flatten before fixation. Secondly, embedding might lead to further shrinkage due to the pressure of the coverslip onto the slice, probably induced by adhesion forces between the coverslip and the embedding material. Third, in acute slices the washout of cell debris from the slice surface is likely to render the uppermost part of the slice more compressible than the deeper tissue. These effects may also cause the reduced visibility of barrel structures in thalamocortical slices after embedding. However, the assumption of linear shrinkage is still a good first-order approximation (Fig. 8*B*), that was used here to estimate the shrinkage-induced distortion of the dendrite-free angle. Accordingly, an increase of the dendrite-free angle of at most ~50° is induced, which cannot invalidate our conclusions regarding the difference between SSNs and SPNs (see Results).

Dendritic Structure of Cell Types and their Location Within Barrels

In accordance with Golgi studies of mouse and rat barrel cortex, the dendritic field of most spiny neurons in L4 displayed a marked asymmetry, being oriented toward the respective barrel center and thus confined to the home barrel (Lorente de Nò 1922; Woolsey et al. 1975; Steffen and Van der Loos 1980; Simons and Woolsey 1984). This symmetry property was quantitatively characterized by the dendrite-free angular section of reconstructed neurons that were projected into the tangential plane of the barrel field. Considerable asymmetry was observed for SSNs, and less so for SPNs. Thus, a spiny L4 barrel neuron with a strongly asymmetric dendritic field is more likely an SSN, whereas lack of asymmetry is more characteristic of SPNs. The strong asymmetry of barrel SSNs differs from the radial symmetry of visual cortex SSNs (Lund 1984; Martin and Whitteridge 1984; Anderson et al. 1994; Hirsch 1995), although moderate asymmetries at borders of ocular dominance columns have been observed (Katz et al. 1989; Kossel et al. 1995). Staiger et al. (2004) also report symmetry properties of L4 neurons in thalamocortical slices in a qualitative manner; although these authors do not observe a cell-type–related bias in symmetry, it may well be that rotation of the neurons into the tangential plane would yield a somewhat different result.

The fairly strong correlation between spiny cell type and symmetry demonstrated here suggests that SPNs are located preferentially within barrel centers, whereas SSNs tend more toward "inhabiting" the barrel walls. The data set based on in vivo fillings clearly shows that this is more a tendency than a strict rule (Fig. 4*E*; see also Sun et al. 2006, their Fig. 1). In particular, we find symmetric SPNs close to the barrel border that extend part of their dendrites into the septa. There is also a subset of symmetric SSNs that was not observed in the thalamocortical slices; this difference may be related to development (P29 vs. P14). Nevertheless, dendrites of most symmetric neurons are also subject to intrabarrel confinement.

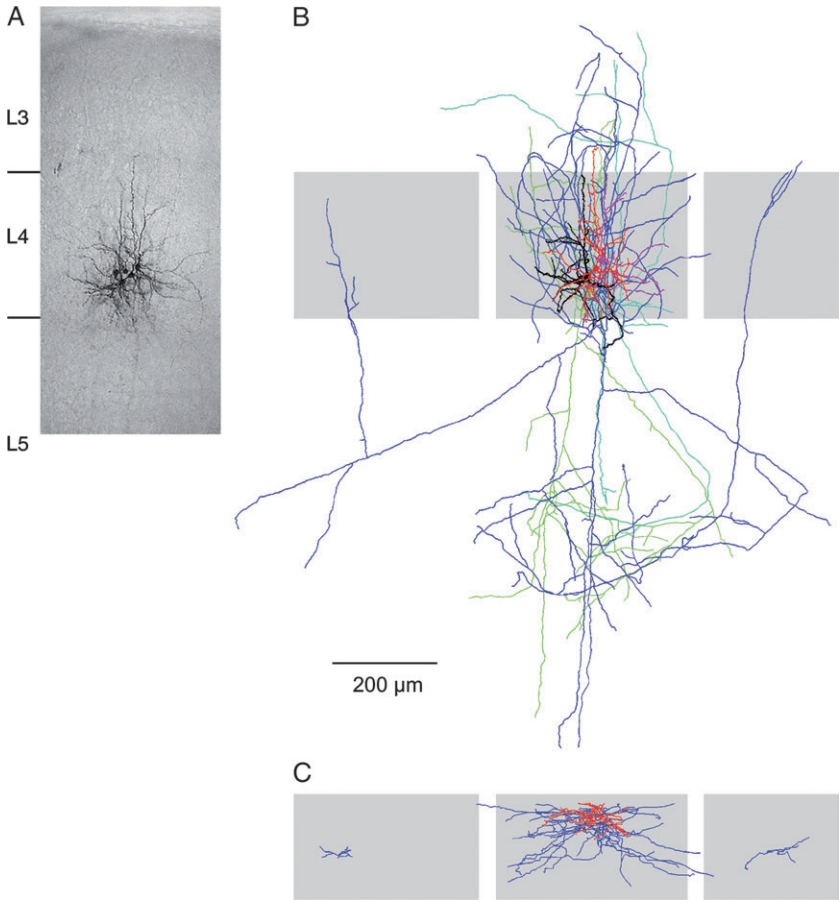

Figure 7. Cluster of SPNs in barrel center, one with interbarrel projection. (*A*) Photo of 5 biocytin-stained neurons in the center of a barrel in a thalamocortical slice, taken at a 10× magnification, cortical layers indicated on the left side. (*B*) Reconstruction of somata, dendrites, and axons of the 3 best-stained neurons. The projection of the dendrites of the red cell into the horizontal plane is shown in the middle of Figure 3*C*. Color scheme: One cell in red (dendrites) and blue (axon collaterals), a second cell in black and green, and a third cell in magenta and turquoise. The projection of the red–blue neuron reaches the centers of 2 adjacent barrels. Schematic barrels are indicated in light gray. Note also the relatively strong collateralization of all star pyramid axon collaterals within lower L5/L6. (*C*) Projection of the red (dendrite) and blue (axon) SPN into the tangential plane with the axon collaterals reduced to L4. Schematic barrels are indicated in light gray. Scale as in (*A*).

Functional Differences between SSNs and SPNs

Are SSNs and SPNs also functionally distinct within the context of the barrel circuitry? As far as known by now from paired recordings from spiny L4 neurons, their synaptic properties do not differ to a large extent (Feldmeyer et al. 1999; but see Cowan and Stricker 2004), and SPNs have been viewed as precursors of SSNs, that evolve by degeneration of the apical dendrite (e.g., Lund 1984; Elston and Rosa 1997). Clearly, our reconstructions represent snapshots at around P14 and P29, respectively, and differences might disappear or increase later on. However, in the adult the general pattern of dendritic intrabarrel confinement is conserved (Woolsey et al. 1975; Steffen and Van der Loos 1980; Greenough and Chang 1988; Tailby et al. 2005), and SPNs are still present (Simons and Woolsey 1984).

Moreover, SPNs have been shown to be integrated in different cortical circuits than the pathways that include SSNs, both in somatosensory and visual cortex. In the barrel cortex, SPNs receive more interbarrel inputs and also more input from other cortical layers within the same barrel column than SSNs (Schubert et al. 2003). In the primate visual cortex, SSNs and SPNs were also found to receive different inputs from L4 sublayers (Yabuta et al. 2001).

As to their primary sensory activation, SSNs and SPNs appear to receive the same type of direct thalamocortical input (Porter et al. 2001; Staiger et al. 2004; Bruno and Sakmann 2006); nevertheless they show different degrees of adaptation to repetitive whisker stimulation in vivo (Brecht and Sakmann 2002a). Cat visual cortex SSNs and SPNs neurons responded similarly to visual input and electrical stimulation of their afferents (Martin and Whitteridge 1984). Differences between the axonal projection patterns of SPNs and SSNs are discussed below.

Axon Arbor Confinement and Overlap with the Dendritic Arbor

The columnar axonal confinement of SSNs and SPNs to the domain of the dendritic tree and thus to the barrel at the level of L4 is rather strict in comparison with similar tendencies observed in monkey visual and somatosensory cortex (Jones 1975; Katz et al. 1989). Moreover, projection patterns of spiny neurons in L4 of visual cortices may vary considerably (e.g., Martin and Whitteridge 1984; Lund et al. 1995; Fitzpatrick 1996; Yabuta and Callaway 1998), whereas they are rather uniform in barrel cortex, possibly indicating a higher degree of complexity of visual cortex circuitry.

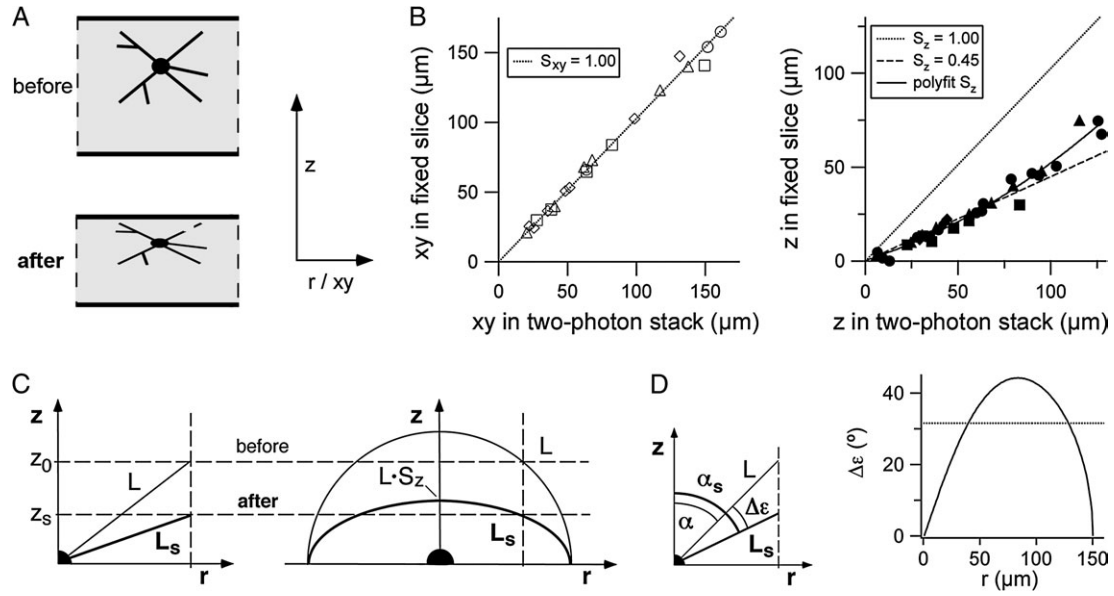

Figure 8. Shrinkage and its influence on the dendrite-free angle. (*A*) Schematic side view of a thalamocortical slice (slice surface top) with a neuron with radially symmetric dendritic field before (top) and after *z*-shrinkage (bottom). This direction of view corresponds to the view onto a neuron after rotation (see also Figs 2, 3). Both the dendrites that enclose the largest dendrite-free angle extend toward the slice surface, yielding a comparatively large shrinkage-induced increase $\Delta\varepsilon$ in dendrite-free angle. The cylindrical coordinate system used for the estimate is indicated on the right, with the *z*-axis perpendicular to the slice surface as before and the *r*-axis being within the *xy*-plane as defined in Figure 3*A* left. (*B*) Measurement of shrinkage in planar direction (*xy*, left panel) and in perpendicular direction (*z*, right panel) relative to the slice surface by comparison of the extent of neuronal structures in the embedded slice (left axes) versus their extent in the 2-photon scan taken in the acute slice (bottom axes; see Methods). The data points are taken from 4 spiny stellate cells, thus 4 symbols. Note the nonlinearity in shrinkage for the perpendicular direction, as seen in the polynomial fit of the data versus their average value $S_z = 0.45$. (*C*) Parameters relevant for shrinkage analysis. Same coordinate system as in (*A*). Thin lines represent the original state, bold lines structures after shrinkage. The soma is schematically indicated at the origin of the coordinate system. Left panel: Influence of *z*-shrinkage on an individual dendrite. The *r*-coordinate of the dendrite is unchanged (marked by vertical broken line), whereas the *z*-coordinate is reduced from z_0 to z_s. Thus, there is a change in the overall length *L* to L_s and also in the angle between dendrite and *z*-axis. Right panel: Influence of *z*-shrinkage on all possible dendritic orientations, as given by the expression for L_s (eq. 1 in Methods). Note that dendrites perpendicular to the *z*-axis are not affected by shrinkage. The broken lines mark the position of the individual dendrite in the left panel. (*D*) Left panel: Parameters relevant for influence of shrinkage on the dendrite-free angle. Coordinates as above in (*B*), bold letters and lines indicating the state after shrinkage. α is the angle between *z*-axis and dendrite before shrinkage, α_s after shrinkage. $\Delta\varepsilon$ is the induced increase in ε, provided the drawn dendrite actually encloses ε. Right panel: Change in dendrite-free angle $\Delta\varepsilon$ as a function of the *r*-coordinate of dendrites enclosing ε, for the case of dendritic orientation shown in (*A*) (eq. 3 in Methods). Horizontal broken line: mean value $<\Delta\varepsilon>$.

We found that spiny L4 neurons display a dense axonal arborization and a strong overlap between their axonal and dendritic domain compared with pyramidal neurons in supra- or infragranular layers. The dense arborization underlies the high intrabarrel connectivity of spiny neurons (~30%; Feldmeyer et al. 1999; Petersen and Sakmann 2000). The overlap is significantly stronger in SSNs than in SPNs, constituting another difference between the 2 neuronal classes. Because the stronger overlap is not due to a larger axonal projection of SSNs at the level of L4 (see Table 2), it appears that SPNs project more diffusely within the barrel. This observation is in line with data from cat visual cortex, where SPNs were observed to project in a more diffuse manner than SSNs; although some SSN projections were found to cluster locally, this was also not observed for SPNs (Martin and Whitteridge 1984). Similarly, Yabuta et al. (2001) investigated SPNs and SSNs in layer 4B of primary visual cortex in the primate and suggested that the 2 cell types were part of 2 functionally separate subsystems, that is, the P and M pathway, also based on their different projection targets.

Taken together with the above observations on different inputs to barrel SSNs and SPNs, these findings suggest that throughout visual and somatosensory cortex the 2 cell types, STPs and SSNs, may be integrated into different circuits that are involved in different computational tasks. It remains to be elucidated what kind of tasks that could be within barrel cortex. Perhaps the relative localization of SSNs closer to the barrel border and their stronger local axo-dendritic overlap as described here might make them more suitable for carrying subcolumnar information (see below), whereas SPNs might be more apt to process information that pertains to the principal whisker as a whole.

Functional Implications of Strong Overlap between Axonal and Dendritic Domains

The asymmetric orientation of SSN dendrites has been suggested to maximize the contact with the segregated afferent thalamocortical projections (Killackey 1973; Arnold et al. 2001). In fact, the activity of the thalamocortical afferents maintains dendritic bias in L4 (Tailby et al. 2005). Because of the strong axonal confinement of SSN and/or SPNs, this input segregation would be further preserved at the level of L4, ensuring that each barrel primarily processes information from its principal whisker (but see below).

Our anatomical observation of a pronounced overlap with the dendrites of the same SSN/SPN promotes recurrent excitation and thus could enhance the responsiveness of barrel neurons. Obviously, the narrow axonal domain will also restrict lateral spread of excitation within a barrel column. Such locally restricted networks on a subbarrel scale strongly imply the existence of coactive subcolumns or perhaps minicolumns within a barrel, as suggested previously (Land and Simons 1985; Yuste et al. 1992; Simons 1995) that may encode for particular receptive field (RF) properties. The strictly columnar projection of SSNs to L2/3 (Lübke et al. 2000, 2003) implies that

any subcolumnar patterns in L4 will be repeated at the level of L2/3.

Indeed, barrel neurons appear to be direction sensitive (e.g., Brecht and Sakmann 2002a) and in addition to exhibit clusters of neurons that are selective for certain directions of whisker deflection, also called angular tuning domains (Simons 1978; Bruno et al. 2003). These domains may be arranged in a stereotypical manner, at least within L2/3 of the D3 barrel, where they would continuously represent the direction toward the next-neighbor whisker (Andermann and Moore 2006). However, according to the in vivo single unit recordings (Bruno et al. 2003), angular tuning domains are at maximum 100 μm in width and thus smaller than the average dendritic field span of SSNs and SPNs, thereby fitting more into the canonic size of minicolumns as suggested by Mountcastle (1978, 1997). It remains to be elucidated whether L4 neurons are indeed organized in direction-selective minicolumns, whether direction selectivity is mapped in a more continuous way and how such minicolumns would be mapped onto the coarse subbarrel structure that was recently revealed (Land and Erickson 2005). Direction-selective RFs could be based on dendritic asymmetry, as suggested for the L6 Meynert cell (Livingstone 1998). However, complex RF properties are usually not found in the primary input regions, and a link between direction selectivity and dendritic asymmetry in the primary visual cortex has been questioned (Anderson et al. 1999; cells L3–6), albeit these neurons display rather weak asymmetry in comparison with spiny barrel neurons. However, dendritic asymmetry in L4 barrel neurons is unlikely to underlie directional tuning, because direction-sensitive responses are observed along the entire whisker input pathway (e.g., Lichtenstein et al. 1990; Brecht and Sakmann 2002b; Minnery and Simons 2003; Timofeeva et al. 2003; Bruno and Sakmann 2006).

Irrespective of the RF properties that may be encoded within minicolumns, the strong recurrent excitation provided by the local axonal projection may also serve to amplify cortical inputs (Feldmeyer et al. 1999), to sustain persistent cortical activity within the barrel (McCormick et al. 2003), or to render the cortical circuits sensitive to synchronous inputs (Pinto et al. 2003).

Interbarrel Connectivity

A small fraction of all neurons from our sample violated the principle of the intrabarrel confinement of axon collaterals, projecting directly into neighboring barrels. These neurons may thus provide direct input to neighboring barrels and therefore represent a substrate for transcolumnar inputs observed in vitro (Schubert et al. 2003) and multiwhisker surround RFs observed in vivo (Fox et al. 2003) that both originated from within layer 4. Due to truncation of axonal processes and insufficient staining the ~5% interbarrel projection neurons reported here represent a lower limit, although thalamocortical slices are oriented along rows, the preferred direction for interbarrel connections (Bernardo et al. 1990; Keller and Carlson 1999). In addition, SPNs were observed to extend their local axonal domain into the adjacent septum as well as the barrels (Staiger et al. 2004). Although these interbarrel projections are unlikely to represent a major pathway of cortical processing within L4, they challenge the view of barrels as entirely independent processing units of thalamic input (Goldreich et al. 1999; Petersen and Sakmann 2001; Laaris and Keller 2002), a notion that is also questioned in relation to subthreshold multiwhisker RFs at the level of individual barrels (reviewed in Moore et al. 1999). Lesions of the spinal trigeminal nucleus interpolaris (SpVi) were found to greatly shrink the thalamic multiwhisker RFs to nearly single-whisker representations and show that, although cortical surround RFs are predominantly thalamocortically generated, there is still some residual surround component to barrel RFs, which may be intracortically mediated (Kwegyir-Afful et al. 2005).

The 2 SSNs shown in Figure 6 display a pronounced interbarrel projection, with an arborization density similar to the intrabarrel projection. Although the database is small, these dense SSN interbarrel projections contrast with the rather weak SPN interbarrel projections (Fig. 7; Brecht and Sakmann 2002a), constituting another difference between the 2 cell types. This clustered SSN projection pattern again supports the hypothesis of functionally segregated subbarrels or minicolumns. Furthermore, these minicolumns may be arranged in a similar fashion across barrels: both interbarrel projections appear to target the same relative barrel segment in the adjacent barrel as the projection in the home barrel. This observation also holds for the 2-week projections into the centers of neighboring barrels by a SPN (Fig. 7). SSNs with patchy projection patterns within L4 have been observed also in visual cortex, for example, in cat striate cortex, suggesting a link between ocular dominance columns from the same eye (Martin and Whitteridge 1984; their Fig. 9), and in monkey primary visual cortex, where intrinsic connections involving SSNs form a periodic lattice within L4B (Rockland and Lund 1983) and a certain subtype of SSN projects to multiple blob regions (Yabuta and Callaway 1998; their Fig. 2*A*). Moreover, lateral axonal projections in visual cortex might generate orientation selectivity in RFs of L2/3 neurons (Lund et al. 1995). Based on measurements of surround-whisker RFs, Armstrong-James et al. (1992) suggested that direct intracortical relays between barrels exist which could allow for feed-forward excitation across barrels for associated whisker deflections, for example, between whiskers that are deflected in the same direction. Thus, the 3 interbarrel projections of spiny L4 neurons documented here might terminate in subcolumnar domains that encode for the same RF property—for example, the whisker-deflection angle—as their axonal and dendritic intrabarrel domains. Taken together, the interbarrel projections documented here likely represent the anatomical substrate for the intracortical component of multiwhisker RFs and may transmit unique subcolumnar information, perhaps including directional tuning, between cortical columns. Rodent barrel cortex thus appears to have complex wiring principles also found in cat and primate primary visual cortex, suggesting a common scheme of cortical organization to process pertinent sensory information.

Notes

The authors would like to thank Prof. B. Sakmann for support, S. Kranz, K. Gari, M. Ebrahimzadeh, N. Belovska, V. Hotz, T. Kurz, R. Masionyte, B. Gärtner, M. März, M. Kurz for performing reconstructions, I. Dehof and M. Kaiser for technical assistance, Dr C. Petersen for help with the tangential slices, Drs M. Brecht, D. Feldmeyer, and E. A. Nimchinsky for comments on the manuscript, and Prof. A. Schüz for valuable hints.
Conflict of Interest: None declared.

Address correspondence to Dr Veronica Egger, Institut für Physiologie der LMU, Pettenkoferstr. 12, 80336 München, Germany. Email: V.Egger@lmu.de.

References

Agmon A, Connors BW. 1991. Thalamocortical responses of mouse somatosensory cortex (barrel cortex) in vitro. Neuroscience. 41:365–379.

Andermann ML, Moore CI. 2006. A somatotopic map of vibrissa motion direction within a barrel column. Nat Neurosci. 9:543–551.

Anderson JC, Binzegger T, Kahana O, Martin KA, Segev I. 1999. Dendritic asymmetry cannot account for directional responses of neurons in visual cortex. Nat Neurosci. 2:820–824.

Anderson JC, Douglas RJ, Martin KA, Nelson JC. 1994. Synaptic output of physiologically identified spiny stellate neurons in cat visual cortex. J Comp Neurol. 341:16–24.

Armstrong-James M, Fox K, Das-Gupta A. 1992. Flow of excitation within rat barrel cortex on striking a single vibrissa. J Neurophysiol. 68:1345–1358.

Arnold PB, Li CX, Waters RS. 2001. Thalamocortical arbors extend beyond single cortical barrels: an in vivo intracellular tracing study in rat. Exp Brain Res. 136:152–168.

Bernardo KL, McCasland JS, Woolsey TA, Strominger RN. 1990. Local intra- and interlaminar connections in mouse barrel cortex. J Comp Neurol. 291:231–255.

Bernardo KL, Woolsey TA. 1987. Axonal trajectories between mouse somatosensory thalamus and cortex. J Comp Neurol. 258: 542–564.

Brecht M, Sakmann B. 2002a. Dynamic representation of whisker deflection by synaptic potentials in spiny stellate and pyramidal cells in the barrels and septa of layer 4 rat somatosensory cortex. J Physiol. 543:49–70.

Brecht M, Sakmann B. 2002b. Whisker maps of neuronal subclasses of the rat ventral posterior medial thalamus, identified by whole-cell voltage recording and morphological reconstruction. J Physiol. 538:495–515.

Bruno RM, Khatri V, Land PW, Simons DJ. 2003. Thalamocortical angular tuning domains within individual barrels of rat somatosensory cortex. J Neurosci. 23:9565–9574.

Bruno RM, Sakmann B. 2006. Cortex is driven by weak but synchronously active thalamocortical synapses. Science. 312:1622–1627.

Cowan AI, Stricker C. 2004. Functional connectivity in layer IV local excitatory circuits of rat somatosensory cortex. J Neurophysiol. 92:2137–2150.

Dodt H-U, Frick A, Kampe K, Zieglgänsberger W. 1998. NMDA and AMPA receptors on neocortical neurons are differentially distributed. Eur J Neurosci. 10:3351–3357.

Elston GN, Rosa MGP. 1997. The occipitoparietal pathway of the macaque monkey: comparison of pyramidal cell morphology in layer III of functionally related cortical visual areas. Cereb Cortex. 7:432–452.

Feldmeyer D, Egger V, Lübke J, Sakmann B. 1999. Reliable synaptic connections between pairs of excitatory layer 4 neurons within a 'barrel' of rat somatosensory cortex. J Physiol (Lond). 521: 169–190.

Fitzpatrick D. 1996. The functional organization of local circuits in visual cortex: insights from the study of tree shrew striate cortex. Cereb Cortex. 6:329–341.

Fleidervish IA, Binshtok AM, Gutnick MJ. 1998. Functionally distinct NMDA receptors mediate horizontal connectivity within layer 4 of mouse barrel cortex. Neuron. 21:1–20.

Fox K, Wright N, Wallace H, Glazewski S. 2003. The origin of cortical surround receptive fields studied in the barrel cortex. J Neurosci. 23:8380–8391.

Goldreich D, Kyriazi HT, Simons DJ. 1999. Functional independence of layer IV barrels in rodent somatosensory cortex. J Neurophysiol. 82:1311–1316.

Greenough WT, Chang FL. 1988. Dendritic pattern formation involves both oriented regression and oriented growth in the barrels of mouse somatosensory cortex. Brain Res. 47:148–152.

Hellwig B. 2000. A quantitative analysis of the local connectivity between pyramidal neurons in layers 2/3 of the rat visual cortex. Biol Cybern. 82:111–121.

Hines ML, Carnevale NT. 1997. The NEURON simulation environment. Neural Comput. 9:1179–1209.

Hirsch JA. 1995. Synaptic integration in layer IV of the ferret striate cortex. J Physiol. 483:183–199.

Horikawa K, Armstrong WE. 1988. A versatile means of intracellular labeling: injection of biocytin and its detection with avidin conjugates. J Neurosci Methods. 25:1–11.

Hübener M, Bolz J. 1992. Relationships between dendritic morphology and cytochrome oxidase compartments in monkey striate cortex. J Comp Neurol. 324:67–80.

Jones EG. 1975. Varieties and distribution of non-pyramidal cells in the somatic sensory cortex of the squirrel monkey. J Comp Neurol. 160:205–267.

Katz LC, Gilbert CD, Wiesel TN. 1989. Local circuits and ocular dominance columns in monkey striate cortex. J Neurosci. 9:1389–1399.

Keller A, Carlson GC. 1999. Neonatal whisker clipping alters intracortical, but not thalamocortical projections, in rat barrel cortex. J Comp Neurol. 412:83–94.

Killackey HP. 1973. Anatomical evidence for cortical subdivisions based on vertically discrete thalamic projections from the ventral posterior nucleus to cortical barrels in the rat. Brain Res. 51:326–331.

Kossel A, Löwel S, Bolz J. 1995. Relationships between dendritic fields and functional architecture in striate cortex of normal and visually deprived cats. J Neurosci. 15:3913–3926.

Kwegyir-Afful EE, Bruno RM, Simons DJ, Keller A. 2005. The role of thalamic inputs in surround receptive fields of barrel neurons. J Neurosci. 25:5926–5934.

Laaris N, Keller A. 2002. Functional independence of layer IV barrels. J Neurophysiol. 87:1028–1034.

Land PW, Erickson SL. 2005. Subbarrel domains in rat somatosensory (S1) cortex. J Comp Neurol. 490:414–426.

Land PW, Simons DJ. 1985. Cytochrome oxidase staining in the rat SmI barrel cortex. J Comp Neurol. 238:225–235.

Leventhal AG, Schall JD. 1983. Structural basis of orientation sensitivity of cat retinal ganglion cells. J Comp Neurol. 220:465–475.

Lichtenstein SH, Carvell GE, Simons DJ. 1990. Responses of rat trigeminal ganglion neurons to movements of vibrissae in different directions. Somatosens Mot Res. 7:47–65.

Livingstone MS. 1998. Mechanisms of direction selectivity in macaque V1. Neuron. 20:509–526.

Lorente de Nò R. 1922. La corteza cerebral del ratòn. Trab Lab Invest Biol. 20:41–78.

Lübke J, Egger V, Sakmann B, Feldmeyer D. 2000. Columnar organization of synaptically coupled excitatory spiny neurons in layer 4 of the rat barrel cortex. J Neurosci. 20:5300–5311.

Lübke J, Roth A, Feldmeyer D, Sakmann B. 2003. Morphometric analysis of the columnar innervation domain of neurons connecting layer 4 and layer 2/3 of juvenile rat barrel cortex. Cereb Cortex. 13:1051–1063.

Lund J. 1984. Cerebral cortex 1. Cellular components of the cerebral cortex. In: Peters A, Jones EG, editors. New York: Plenum Press. p. 255–307.

Lund JS, Wu Q, Hadingham PT, Levitt JB. 1995. Cells and circuits contributing to functional properties in area V1 of macaque monkey cerebral cortex: bases for neuroanatomically realistic models. J Anat. 187:563–581.

Martin KAC, Whitteridge D. 1984. Form, function and intracortical projections of spiny neurones in the striate visual cortex of the cat. J Physiol (Lond). 353:463–504.

McCormick DA, Shu Y, Hasenstaub A, Sanchez-Vives M, Badoual M, Bal T. 2003. Persistent cortical activity: mechanisms of generation and effects on neuronal excitability. Cereb Cortex. 13:1219–1231.

Minnery BS, Simons DJ. 2003. Response properties of whisker-associated trigeminothalamic neurons in rat nucleus principalis. J Neurophysiol. 89:40–56.

Mizrahi A, Ben-Ner E, Katz MJ, Kedem K, Glusman JG, Libersat F. 2000. Comparative analysis of dendritic architecture of identified neurons using the Hausdorff distance metric. J Comp Neurol. 422:415–428.

Moore CI, Nelson SB, Sur M. 1999. Dynamics of neuronal processing in rat somatosensory cortex. Trends Neurosci. 22:513–520.

Mountcastle VB. 1978. An organizing principle for cerebral function. In: Edelman GM, Mountcastle VB, editors. The mindful brain. Cambridge (MA): MIT Press. p. 7–50.

Mountcastle VB. 1997. The columnar organization of the neocortex. Brain. 120:701–722.
Nevian T, Sakmann B. 2006. Spine Ca^{2+} signaling in spike-timing dependent plasticity. J Neurosci. 26:11001–11013.
Petersen CCH, Sakmann B. 2000. The excitatory neuronal network of layer 4 barrel cortex. J Neurosci. 20:7579–7586.
Petersen CCH, Sakmann B. 2001. Functionally independent columns of rat somatosensory barrel cortex revealed with voltage-sensitive dye imaging. J Neurosci. 21:8435–8446.
Pinto DJ, Hartings JA, Brumberg JC, Simons DJ. 2003. Cortical damping: analysis of thalamocortical response transformations in rodent barrel cortex. Cereb Cortex. 13:33–44.
Porter JT, Johnson CK, Agmon A. 2001. Diverse types of interneurons generate thalamus-evoked feedforward inhibition in the mouse barrel cortex. J Neurosci. 21:2699–2710.
Rockland KS, Lund JS. 1983. Intrinsic laminar lattice connections in primate visual cortex. J Comp Neurol. 216:303–318.
Schubert D, Kotter R, Zilles K, Luhmann HJ, Staiger JF. 2003. Cell type-specific circuits of cortical layer IV spiny neurons. J Neurosci. 23:2961–2970.
Sholl DA. 1953. Dendritic organization in the neurons of the visual and motor cortices of the cat. J Anat. 87:387–407.
Simons DJ. 1978. Response properties of vibrissa units in rat SI somatosensory neocortex. J Neurophysiol. 41:798–820.
Simons DJ. 1995. Neuronal integration in the somatosensory whisker/barrel cortex. Cereb Cortex. 11:263–293.
Simons DJ, Woolsey TA. 1984. Morphology of Golgi-Cox-impregnated barrel neurons in rat SmI cortex. J Comp Neurol. 230: 119–132.
Staiger JF, Flagmeyer I, Schubert D, Zilles K, Kotter R, Luhmann HJ. 2004. Functional diversity of layer IV spiny neurons in rat somatosensory cortex: quantitative morphology of electrophysiologically characterized and biocytin labeled cells. Cereb Cortex. 14:690–701.
Steffen H, Van der Loos H. 1980. Early lesions of mouse vibrissal follicles: their influence on dendrite orientation in the cortical barrelfield. Exp Brain Res. 40:419–431.
Sun Q-Q, Huguenard JR, Prince DA. 2006. Barrel cortex microcircuits: thalamocortical feedforward inhibition is mediated by a small number of fast-spiking interneurons. J Neurosci. 26:1219–1230.
Tailby C, Wright LL, Metha AB, Calford MB. 2005. Activity-dependent maintenance and growth of dendrites in adult cortex. Proc Natl Acad Sci U S A. 102:4631–4636.
Timofeeva E, Merette C, Emond C, Lavallee P, Deschenes M. 2003. A map of angular tuning preference in thalamic barreloids. J Neurosci. 23:10717–10723.
Wong-Riley M. 1979. Changes in the visual system of monocularly sutured or enucleated cats demonstrable with cytochrome oxidase histochemistry. Brain Res. 171:11–28.
Wong-Riley MT, Welt C. 1980. Histochemical changes in cytochrome oxidase of cortical barrels after vibrissal removal in neonatal and adult mice. Proc Natl Acad Sci U S A. 77:2233–2237.
Woolsey TA, Dierker ML, Wann DF. 1975. Mouse SmI cortex: qualitative and quantitative classification of Golgi-impregnated barrel neurons. Proc Natl Acad Sci U S A. 72:2165–2169.
Yabuta NH, Callaway EM. 1998. Functional streams and local connections of layer 4C neurons in primary visual cortex of the macaque monkey. J Neurosci. 18:9489–9499.
Yabuta NH, Sawatari A, Callaway EM. 2001. Two functional channels from primary visual cortex to dorsal visual cortical areas. Science. 292:297–300.
Yuste R, Peinado A, Katz LC. 1992. Neuronal domains in developing neocortex. Science. 257:665–669.